First demonstration of long-haul transmission using silicon microring modulators

Aleksandr Biberman,[1,*] Sasikanth Manipatruni,[2,*] Noam Ophir,[1] Long Chen,[2] Michal Lipson,[2,3] and Keren Bergman[1]

[1]*Department of Electrical Engineering, Columbia University, New York, New York, USA*
[2]*School of Electrical and Computer Engineering, Cornell University, Ithaca, New York, USA*
[3]*Kavli Institute at Cornell, Ithaca, New York, USA*
biberman@ee.columbia.edu
[*]*These authors contributed equally to this work.*

Abstract: We report error-free long-haul transmission of optical data modulated using a silicon microring resonator electro-optic modulator with modulation rates up to 12.5 Gb/s. Using bit-error-rate and power penalty characterizations, we evaluate the performance of this device with varying modulation rates, and perform a comparative analysis using a commercial electro-optic modulator. We then experimentally measure the signal integrity degradation of the high-speed optical data with increasing propagation distances, induced chromatic dispersions, and bandwidth-distance products, showing error-free transmission for propagation distances up to 80 km. These results confirm the functional ubiquity of this silicon modulator, establishing the potential role of silicon photonic interconnects for chip-scale high-performance computing systems and memory access networks, optically-interconnected data centers, as well as high-performance telecommunication networks spanning large distances.

OCIS codes: (250.3140) Integrated optoelectronic circuits; (250.4110) Modulators; (130.0250) Optoelectronics; (230.3120) Integrated optics devices.

References and links

1. I. A. Young, E. Mohammed, J. T. S. Liao, A. M. Kern, S. Palermo, B. A. Block, M. R. Reshotko, and P. L. D. Chang, "Optical I/O technology for tera-scale computing," IEEE J. Solid-State Circuits **45,** 235–248 (2010).
2. D. A. B. Miller, "Device requirements for optical interconnects to silicon chips," Proc. IEEE **97,** 1166–1185 (2009).
3. A. V. Krishnamoorthy, R. Ho, X. Zheng, H. Schwetman, J. Lexau, P. Koka, G. Li, I. Shubin, and J. E. Cunningham, "Computer systems based on silicon photonic interconnects," Proc. IEEE **97,** 1337–1361 (2009).
4. C. Batten, A. Joshi, J. Orcutt, A. Khilo, B. Moss, C. W. Holzwarth, M. A. Popović, H. Li, H. I. Smith, J. L. Hoyt, F. X. Kärtner, R. J. Ram, V. Stojanović, and K. Asanović, "Building many-core processor-to-DRAM networks with monolithic CMOS silicon photonics," IEEE Micro **29,** 8–21 (2009).
5. R. G. Beausoleil, J. Ahn, N. Binkert, A. Davis, D. Fattal, M. Fiorentino, N. P. Jouppi, M. McLaren, C. M. Santori, R. S. Schreiber, S. Spillane, D. Vantrease, and Q. Xu, "A nanophotonic interconnect for high-performance many-core computation," Proc. Integrated Photonics and Nanophotonics Research and Applications (IPNRA), ITuD2 (2008).
6. A. Shacham, K. Bergman, and L. P. Carloni, "On the design of a photonic network-on-chip," Proc. International Symposium on Networks-on-Chip (NOCS), 53–64 (2007).
7. N. Kirman, M. Kirman, R. K. Dokania, J. F. Martinez, A. B. Apsel, M. A. Watkins, and D. H. Albonesi, "Leveraging optical technology in future bus-based chip multiprocessors," Proc. International Symposium on Microarchitecture (MICRO), 492–503 (2006).
8. A. Narasimha, B. Analui, E. Balmater, A. Clark, T. Gal, D. Guckenberger, S. Gutierrez, M. Harrison, R. Ingram, R. Koumans, D. Kucharski, K. Leap, Y. Liang, A. Mekis, S. Mirsaidi, M. Peterson, T. Pham, T. Pinguet, D. Rines, V. Sadagopan, T. J. Sleboda, D. Song, Y. Wang, B. Welch, J. Witzens, S. Abdalla, S. Gloeckner, and P. Dobbelaere, "A 40-Gb/s QSFP optoelectronic transceiver in a 0.13µm CMOS silicon-on-insulator technology," Proc. Optical Fiber Communication Conference (OFC), OMK7 (2008).

#129651 - $15.00 USD Received 7 Jun 2010; revised 28 Jun 2010; accepted 28 Jun 2010; published 7 Jul 2010

9. X. Zheng, J. Lexau, Y. Luo, H. Thacker, T. Pinguet, A. Mekis, G. Li, J. Shi, P. Amberg, N. Pinckney, K. Raj, R. Ho, J. E. Cunningham, and A. V. Krishnamoorthy, "Ultra-low-energy all-CMOS modulator integrated with driver," Opt. Express **18,** 3059–3070 (2010).
10. B. Schmidt, Q. Xu, J. Shakya, S. Manipatruni, and M. Lipson, "Compact electro-optic modulator on silicon-on-insulator substrates using cavities with ultra-small modal volumes," Opt. Express **15,** 3140–3148 (2007).
11. M. R. Watts, D. C. Trotter, R. W. Young, and A. L. Lentine, "Ultralow power silicon microdisk modulators and switches," Proc. International Conference on Group IV Photonics (GFP), WA2 4–6 (2008).
12. S. Manipatruni, L. Chen, K. Preston, and M. Lipson, "Ultra low power electro-optic modulator on silicon: towards direct logic driven silicon modulators," Proc. Conference on Lasers and Electro-Optics (CLEO), CThJ6 (2010).
13. L. Liao, A. Liu, D. Rubin, J. Basak, Y. Chetrit, H. Nguyen, R. Cohen, N. Izhaky, and M. Paniccia, "40 Gbit/s silicon optical modulator for high-speed applications," Electron. Lett. **43,** 1196–1197 (2007).
14. S. Manipatruni, Q. Xu, B. Schmidt, J. Shakya, and M. Lipson, "High speed carrier injection 18 Gb/s silicon micro-ring electro-optic modulator," Proc. Annual Meeting of the Lasers and Electro-Optics Society (LEOS), WO2 537–538 (2007).
15. L. Zhou and A. W. Poon, "Silicon electro-optic modulators using p-i-n diodes embedded 10-micron-diameter microdisk resonators," Opt. Express **14,** 6851–6857 (2006).
16. C. Gunn, "CMOS photonics™ - SOI learns a new trick," Proc. International Silicon-on-Insulator Conference (SOI), 7–13 (2005).
17. P. Dong, S. Liao, D. Feng, H. Liang, D. Zheng, R. Shafiiha, C.-C. Kung, W. Qian, G. Li, X. Zheng, A. V. Krishnamoorthy, and M. Asghari, "Low V_{pp}, ultralow-energy, compact, high-speed silicon electro-optic modulator," Opt. Express **17,** 22484–22490 (2009).
18. J. Zhang, T.-Y. Liow, G.-Q. Lo, and D.-L. Kwong, "10Gbps monolithic silicon FTTH transceiver without laser diode for a new PON configuration," Opt. Express **18,** 5135–5141 (2010).
19. Y. Goebuchi, T. Kato, and Y. Kokubun, "Fast and stable wavelength-selective switch using double-series coupled dielectric microring resonator," IEEE Photon. Technol. Lett. **18,** 538–540 (2006).
20. M. A. Popović, T. Barwicz, F. Gan, M. S. Dahlem, C. W. Holzwarth, P. T. Rakich, H. I. Smith, E. P. Ippen, and F. X. Kärtner, "Transparent wavelength switching of resonant filters," Proc. Conference on Lasers and Electro-Optics (CLEO), CPDA2 (2007).
21. H. L. R. Lira, S. Manipatruni, and M. Lipson, "Broadband hitless silicon electro-optic switch for on-chip optical networks," Opt. Express **17,** 22271–22280 (2009).
22. J. Van Campenhout, W. M. J. Green, S. Assefa, and Y. A. Vlasov, "Low-power, 2×2 silicon electro-optic switch with 110-nm bandwidth for broadband reconfigurable optical networks," Opt. Express **17,** 24020–24029 (2009).
23. G. Dehlinger, S. J. Koester, J. D. Schaub, J. O. Chu, Q. C. Ouyang, and A. Grill, "High-speed germanium-on-SOI lateral PIN photodiodes," IEEE Photon. Technol. Lett. **16,** 2547–2549 (2004).
24. M. Jutzi, M. Berroth, G. Wöhl, M. Oehme, and E. Kasper, "Ge-on-Si vertical incidence photodiodes with 39-GHz bandwidth," IEEE Photon. Technol. Lett. **17,** 1510–1512 (2005).
25. J. Liu, D. D. Cannon, K. Wada, Y. Ishikawa, S. Jongthammanurak, D. T. Danielson, J. Michel, and L. C. Kimerling, "Tensile strained Ge p-i-n photodetectors on Si platform for C and L band telecommunications," Appl. Phys. Lett. **87,** 011110-1–011110-3 (2005).
26. M. Rouvière, M. Halbwax, J.-L. Cercus, E. Cassan, L. Vivien, D. Pascal, M. Heitzmann, J.-M. Hartmann, and S. Laval, "Integration of germanium waveguide photodetectors for intrachip optical interconnects," Opt. Eng. **44,** 075402-1–075402-5 (2005).
27. L. Colace, G. M. A. Altieri, and G. Assanto, "Waveguide photodetectors for the near-infrared in polycrystalline germanium on silicon," IEEE Photon. Technol. Lett. **18,** 1094–1096 (2006).
28. D. Ahn, C.-Y. Hong, J. Liu, W. Giziewicz, M. Beals, L. C. Kimerling, J. Michel, J. Chen, and F. X. Kärtner, "High performance, waveguide integrated Ge photodetectors," Opt. Express **15,** 3916–3921 (2007).
29. L. Vivien, M. Rouvière, J.-M. Fédéli, D. Marris-Morini, J.-F. Damlencourt, J. Mangeney, P. Crozat, L. El Melhaoui, E. Cassan, X. Le Roux, D. Pascal, and S. Laval, "High speed and high responsivity germanium photodetector integrated in a silicon-on-insulator microwaveguide," Opt. Express **15,** 9843–9848 (2007).
30. T. Yin, R. Cohen, M. M. Morse, G. Sarid, Y. Chetrit, D. Rubin, and M. J. Paniccia, "31GHz Ge n-i-p waveguide photodetectors on silicon-on-insulator substrate," Opt. Express **15,** 13965–13971 (2007).
31. L. Chen, P. Dong, and M. Lipson, "High performance germanium photodetectors integrated on submicron silicon waveguides by low temperature wafer bonding," Opt. Express **16,** 11513–11518 (2008).
32. S. Assefa, F. Xia, S. W. Bedell, Y. Zhang, T. Topuria, P. M. Rice, and Y. A. Vlasov, "CMOS-integrated high-speed MSM germanium waveguide photodetector," Opt. Express **18,** 4986–4999 (2010).
33. L. Zhang, Y. Li, J.-Y. Yang, M. Song, R. G. Beausoleil, and A. E. Willner, "Silicon-based microring resonator modulators for intensity modulation," IEEE Select. Topics Quant. Electron. **16,** 149–158 (2010).
34. A. Biberman, N. Ophir, K. Bergman, S. Manipatruni, L. Chen, and M. Lipson, "First demonstration of 80-km long-haul transmission of 12.5-Gb/s data using silicon microring resonator electro-optic modulator," Proc. Optical Fiber Communication Conference (OFC), JWA28 (2010).

#129651 - $15.00 USD Received 7 Jun 2010; revised 28 Jun 2010; accepted 28 Jun 2010; published 7 Jul 2010

35. W. A. Zortman, A. L. Lentine, M. R. Watts, and D. C. Trotter, "Power penalty measurement and frequency chirp extraction in silicon microdisk resonator modulators," Proc. Optical Fiber Communication Conference (OFC), OMI7 (2010).
36. S. Beamer, C. Sun, Y.-J. Kwon, A. Joshi, C. Batten, V. Stojanović, and K. Asanović, "Re-architecting DRAM memory systems with monolithically integrated silicon photonics," Proc. International Symposium on Computer Architecture (ISCA), (2010).
37. J. Chan, G. Hendry, A. Biberman, and K. Bergman, "Architectural exploration of chip-scale photonic interconnection network designs using physical-layer analysis," J. Lightwave Technol. **28,** 1305–1315 (2010).
38. S. Manipatruni, L. Chen, and M. Lipson, "50 Gbit/s wavelength division multiplexing using silicon microring modulators," Proc. International Conference on Group IV Photonics (GFP), FC3 244–246 (2009).

1. Introduction

Silicon photonics is recently emerging as a promising solution for bandwidth and energy challenges of future interconnects [1–7], touting compatibility with existing complementary metal-oxide-semiconductor (CMOS) fabrication processes [1,3,8,9], capability of large-scale integration with advanced microelectronics [1,3], ultra-small footprints [10–12], and low power consumption [9–12]. Silicon photonics is slated to deliver orders-of-magnitude performance improvements in both bandwidth and power consumption by interconnecting chip-scale high-performance computing systems and memory access networks, as well as augmenting data center interconnection networks. Many high-performance silicon photonic devices such as modulators [9–19], switches [11,20–22], and germanium-integrated photodetectors [1,23–32], have already been demonstrated for use in interconnection networks. However, the functionalities of silicon photonics for medium- and long-haul optical communications remain largely unexplored [33–35]. In this work, we characterize a high-performance silicon microring resonator electro-optic modulator, and determine its feasibility for use in both medium- and long-haul optical communication networks.

We demonstrate, for the first time to our knowledge, error-free operation of a silicon microring resonator electro-optic modulator for modulation rates up to 12.5 Gb/s, and draw a comparison of this device with a commercial lithium niobate ($LiNbO_3$) Mach-Zehnder electro-optic modulator. To date, all proposed silicon photonic network-on-chip (NoC) architectures have employed silicon microring resonator modulators [1,3–7]. The measurements demonstrated in this work may enable more accurate physical layer modeling of these photonic devices for optically-interconnected high-performance computing systems [36,37].

In this work, to the best of our knowledge, we also present the first experimental demonstration of an error-free long-haul (up to 80-km) transmission using a high-speed (up to 12.5-Gb/s) and compact (12-μm diameter) silicon microring modulator, demonstrating a bandwidth-distance product up to 1000 Gb-km/s. We experimentally measure less than a 1-dB power penalty associated with the bandwidth-distance product of 600 Gb-km/s, comparable to commercial telecommunications-grade modulators. We also perform bit-error-rate (BER) and power penalty characterizations for varying propagation distances, induced chromatic dispersions, and bandwidth-distance products.

2. Silicon microring resonator electro-optic modulator

The silicon microring resonator electro-optic modulator in this work comprises a microring resonator configured as a PIN carrier injection device [14]. The microring resonator has a 12-μm diameter, optical quality factor of about 10,000, and is coupled to a straight waveguide with input and output ports (Fig. 1d). The waveguides are 450-nm wide and 260-nm tall. The waveguide of the microring has a 50-nm slab that is doped to form the PIN diode structure, with nickel silicide for the electrical contacts. The silicon modulator was fabricated using electron-beam lithography and reactive-ion etching [38]. The non-return-to-zero (NRZ) on-off-keyed (OOK) modulation signal is electro-optically encoded onto a wavelength channel

#129651 - $15.00 USD Received 7 Jun 2010; revised 28 Jun 2010; accepted 28 Jun 2010; published 7 Jul 2010

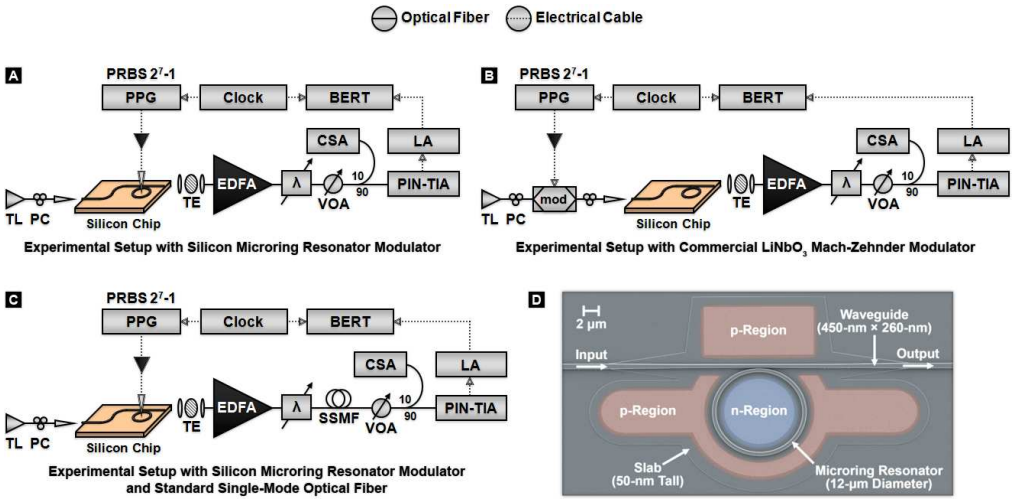

Fig. 1. Experimental setup diagrams for measuring system-level performance of the silicon microring resonator electro-optic modulator. (a) Experimental setup for characterizing the performance of the silicon modulator for modulation rates between 5 and 12.5 Gb/s. (b) Experimental setup for comparative analysis of the silicon modulator using a commercial $LiNbO_3$ Mach-Zehnder electro-optic modulator. (c) Experimental setup for propagating an optical signal encoded using the silicon modulator through varying lengths of standard single-mode optical fiber, between 0 and 80 km, for modulation rates between 10 and 12.5 Gb/s. (d) Top-view scanning-electron-microscope (SEM) image of the silicon modulator.

when an incoming continuous wave (CW) source passes in and out of a shifting resonance of the microring resonator. When the resonance of the microring resonator is tuned onto the wavelength of the incoming signal, the light is coupled into the microring resonator, corresponding to a logical "0" bit. When the resonance of the microring resonator is tuned away from the wavelength of the incoming signal, the signal bypasses the microring resonator and leaves on the output port, corresponding to a logical "1" bit. The resonance shift is induced by the plasma-dispersion effect from injecting and extracting electrical carriers through the PIN diode, which is integrated into the microring resonator. To achieve high modulation rates that are typically limited by carrier lifetimes, the modulator is driven using a pre-emphasis method [1,14].

3. Experimental setup

The experimental setup for characterizing the modulation rate dependence of the silicon microring modulator (Fig. 1a) involves a tunable laser (TL) source generating a CW 1565-nm lightwave that is coupled on chip using a tapered fiber. The lightwave is then modulated on chip using the microring resonator, which is driven by a pulse pattern generator (PPG) generating a 2^7–1 pseudo-random bit sequence (PRBS), followed by a pre-emphasis circuit. Off chip, the signal passes through an erbium-doped fiber amplifier (EDFA), a tunable grating filter (λ), and a variable optical attenuator (VOA). The signal is received by a high-speed PIN photodiode and transimpedance amplifier (PIN-TIA) receiver followed by a limiting amplifier (LA), and is evaluated using a BER tester (BERT). Both the PPG and the BERT are synchronized to the same clock. Using a power tap, a communications signal analyzer (CSA) is used to examine the temporal response of the signal before the receiver. Polarization controllers (PCs) are used throughout the setup. We actively modulate the microring resonator with a 2.5-V_{PP} electrical signal with about a 1-V voltage bias.

The experimental setup for comparing the performance of the silicon modulator with a commercial $LiNbO_3$ Mach-Zehnder electro-optic modulator is similar to the aforementioned experimental setup, except the modulation occurs off chip using the $LiNbO_3$ modulator, before the optical signal is coupled on chip (Fig. 1b). Once on chip, this modulated signal passes by the silicon microring resonator off resonance.

#129651 - $15.00 USD Received 7 Jun 2010; revised 28 Jun 2010; accepted 28 Jun 2010; published 7 Jul 2010

In order to inspect the signal integrity degradation induced by chromatic dispersion effects, the lightwave is again modulated on chip using the microring resonator. Off chip, the signal passes through an EDFA and a tunable grating filter (λ) before passing through varying lengths of standard single-mode optical fiber (SSMF), set to 1-, 2-, 5-, 10-, 15-, 40-, 60-, and 80-km lengths, as well as the 0-km back-to-back case bypassing the optical fiber. After leaving the optical fiber, the signal travels through a VOA, is received by a high-speed PIN-TIA receiver followed by a LA, and is evaluated using a BERT. Again, both the PPG and the BERT are synchronized to the same clock, which is now set to either 10 or 12.5 GHz. Using a power tap, a CSA is used to examine the temporal response of the signal before the receiver. Here, the pre-emphasis circuit is optimized for each modulation rate, and is then kept constant for the varying transmission configurations of propagation distance.

4. Experimental validation of modulation rate and comparative analysis

Using the experimental setup depicted in Fig. 1a and described in the experimental setup section, we first evaluate the silicon modulator at varying modulation rates by examining the output modulation temporal response. This is accomplished by setting the clock rate to 5, 7.5, 10, and 12.5 GHz, electrically driving the silicon modulator with 5-, 7.5-, 10-, and 12.5-Gb/s NRZ OOK data. The electro-optic response of the silicon modulator then encodes the incoming light with the electrical data. Once that data signal leaves the chip, the eye diagrams of the optical signals are measured (Fig. 2a–d). The resulting eye diagrams show clear openings, and degrade as we drive the modulator at higher modulation rates, resulting from electrical carrier lifetime limitations as well as the transient response of the microring resonator and the closing of the temporal window. The pre-emphasis circuit to enable carrier injection and extraction is optimized separately for each modulation rate.

For each modulation rate configuration of the silicon modulator, we perform BER measurements of the resulting optical data signal leaving the chip (Fig. 3a). We first observe error-free operation (defined as having BERs less than 10^{-12}) for each configuration. Subsequently, BER curves are recorded for the 5-, 7.5-, 10-, and 12.5-Gb/s modulation rates. The experimentally-measured BER curves confirm the signal integrity degradation as the modulation rate is increased.

Using the experimental setup depicted in Fig. 1b and described in the experimental setup section, we compare the performance of the silicon modulator with a commercial $LiNbO_3$ Mach-Zehnder electro-optic modulator at varying modulation rates. This is accomplished by setting the clock rate to 5, 7.5, 10, and 12.5 GHz, electrically driving the $LiNbO_3$ modulator with 5-, 7.5-, 10-, and 12.5-Gb/s data. The electro-optic response of the $LiNbO_3$ modulator then encodes the incoming light with this data. The resulting optical data signal is then inserted into the silicon chip, bypassing the microring resonator. Once the data signal leaves the silicon chip, the eye diagrams of the optical signal are evaluated (Fig. 2e–h). The resulting eye diagrams show clear openings, and degrade as we drive the modulator at higher modulation rates, resulting mostly from the closing of the temporal window. The modulation bias is optimized for each configuration. For each modulation rate configuration of the $LiNbO_3$ modulator, we perform BER measurements of the resulting optical data signal leaving the silicon chip (Fig. 3a). We observe error-free operation for each modulation rate, and subsequently record BER curves for the 5-, 7.5-, 10-, and 12.5-Gb/s modulation rates. Again, the experimentally-measured BER curves confirm the signal integrity degradation as the modulation rate is increased.

To draw a system-level functional comparison between the two modulators, the BER curves measured for the $LiNbO_3$ modulator are set as the back-to-back cases for the BER curves measured for the silicon modulator at each modulation rate. The resulting power penalties of the operation of the silicon modulator compared to the $LiNbO_3$ modulator are 1.2, 1.65, 3.15, and 5.4 dB for 5-, 7.5-, 10-, and 12.5-Gb/s modulation rates, respectively, at the BER of 10^{-9} (Fig. 3b). Much of these power penalties may be further improved with more optimal pre-emphasis configurations for each modulation rate, as well as closer integration of the electrical driving circuit with the silicon modulator [1].

#129651 - $15.00 USD Received 7 Jun 2010; revised 28 Jun 2010; accepted 28 Jun 2010; published 7 Jul 2010

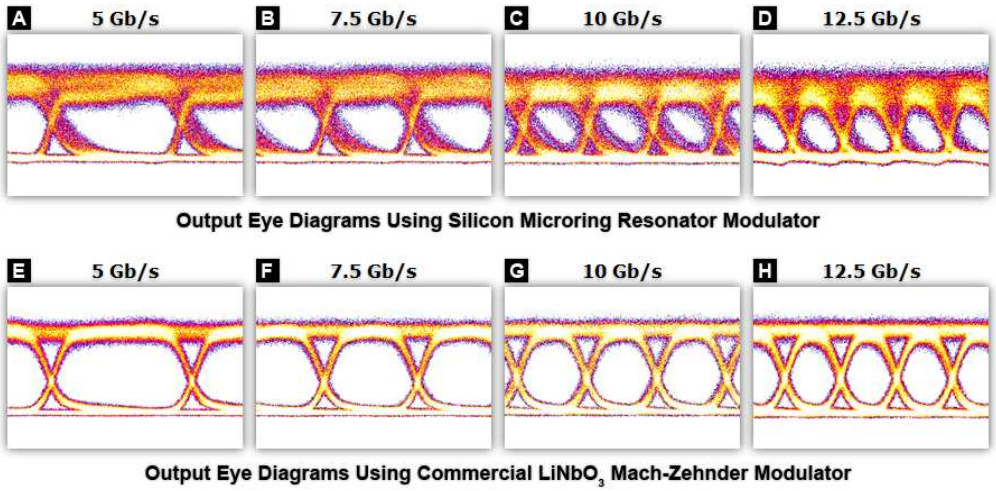

Fig. 2. Experimentally-measured temporal responses of varying modulation rates for the silicon microring resonator electro-optic modulator as well as a commercial $LiNbO_3$ Mach-Zehnder electro-optic modulator. Output eye diagrams for the (a) 5-Gb/s, (b) 7.5-Gb/s, (c) 10-Gb/s, and (d) 12.5-Gb/s modulation rates using the silicon modulator, and (e) 5-Gb/s, (f) 7.5-Gb/s, (g) 10-Gb/s, and (h) 12.5-Gb/s modulation rates using the $LiNbO_3$ modulator.

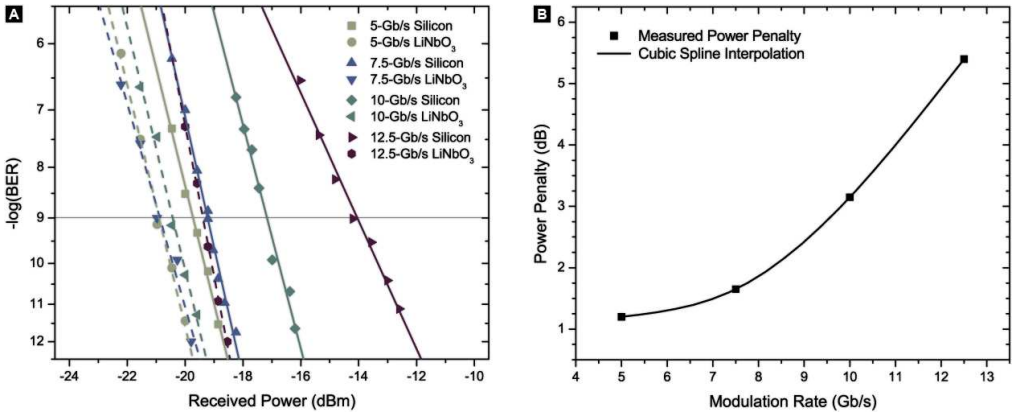

Fig. 3. Experimentally-measured system-level performance characterizations of the silicon microring resonator electro-optic modulator for modulation rates between 5 and 12.5 Gb/s. (a) Bit-error-rate curves for an optical signal encoded using the silicon modulator, as well as a commercial $LiNbO_3$ Mach-Zehnder electro-optic modulator, for 5-, 7.5-, 10-, and 12.5-Gb/s modulation rates. (b) Resulting power penalty associated with the operation of the silicon modulator compared to the $LiNbO_3$ modulator for modulation rates between 5 and 12.5 Gb/s.

5. Experimental evaluation of long-haul transmission

Using the experimental setup depicted in Fig. 1c and described in the experimental setup section, we study the signal integrity degradation induced by the chromatic dispersion effects caused by varying propagation distances through SSMF, resulting from the induced chirp in the silicon modulator. We first transmit a 10-Gb/s modulated signal through SSMF lengths of 0, 1, 2, 5, 10, 15, 40, 60, and 80 km, inducing proportional amounts of chromatic dispersion. The eye diagrams of the resulting optical signals are evaluated for each configuration (Fig. 4a–i). The eye diagrams show clear openings, and remain relatively unchanged for optical fiber lengths up to 15 km (Fig. 4a–f). The eye diagrams subsequently begin to lose temporal window and display increased noise after 40-km propagation distances, as dispersion effects become more distinct (Fig. 4g), displaying noticeable degradation at 60 and 80 km (Fig. 4h,i). To evaluate this dependence of the signal integrity degradation on modulation rate, the silicon

#129651 - $15.00 USD Received 7 Jun 2010; revised 28 Jun 2010; accepted 28 Jun 2010; published 7 Jul 2010

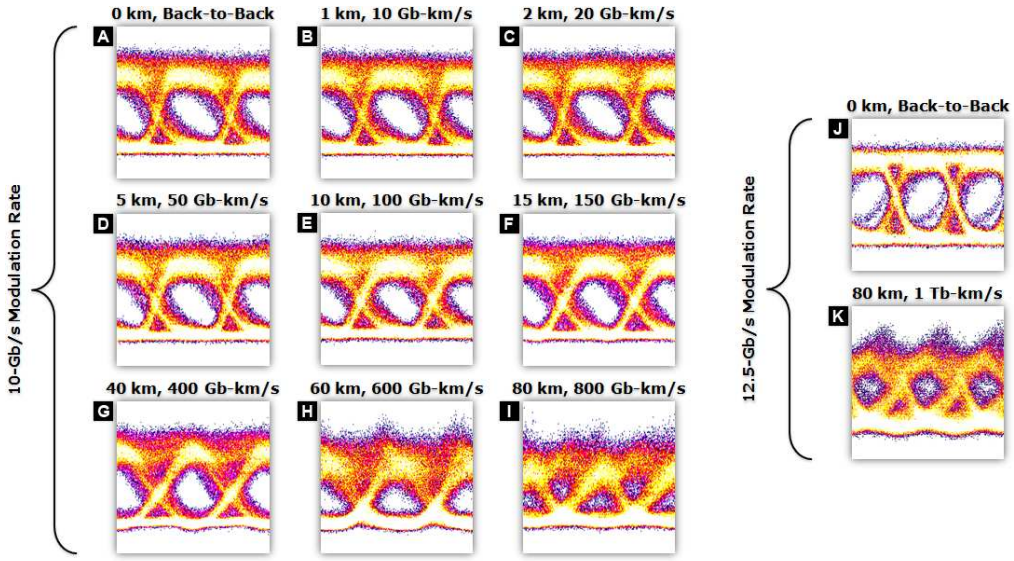

Fig. 4. Experimentally-measured temporal responses of varying propagation distances through standard single-mode optical fiber of an optical signal encoded using the silicon microring resonator electro-optic modulator. Output eye diagrams for the (a) 0-km, (b) 1-km, (c) 2-km, (d) 5-km, (e) 10-km, (f) 15-km, (g) 40-km, (h) 60-km, and (i) 80-km propagation distances for 10-Gb/s modulation rates, as well as (j) 0-km and (k) 80-km propagation distances for 12.5-Gb/s modulation rate, using the silicon modulator.

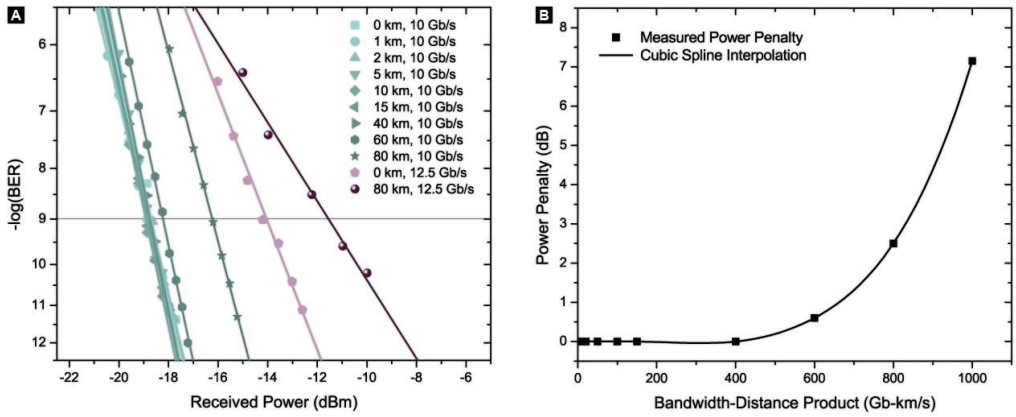

Fig. 5. Experimentally-measured system-level performance characterizations of varying propagation distances through standard single-mode optical fiber of an optical signal encoded using the using the silicon microring resonator electro-optic modulator. (a) Bit-error-rate curves for 0-, 1-, 2-, 5-, 10-, 15-, 40-, 60-, and 80-km propagation distances for 10-Gb/s modulation rates, as well as 0- and 80-km propagation distances for 12.5-Gb/s modulation rates, using the silicon modulator. (b) Resulting power penalty associated with propagating the optical signal encoded using the silicon modulator through varying lengths of standard single-mode optical fiber for 10-Gb/s modulation rate.

modulator is subsequently evaluated at a 12.5-Gb/s modulation rate for the 0- and 80-km optical fiber lengths (Fig. 4j,k). After this 80-km transmission, the eye diagram of the resulting optical signal is evaluated (Fig. 4k). Again, the eye diagram shows noticeable degradation from the induced chromatic dispersion.

We then quantify the signal integrity degradation caused by the chromatic dispersion effects induced by long-haul propagation using BER measurements at varying propagation

#129651 - $15.00 USD Received 7 Jun 2010; revised 28 Jun 2010; accepted 28 Jun 2010; published 7 Jul 2010

Propagation Distance (km)	Modulation Rate (Gb/s)	Induced Chromatic Dispersion (ps/nm)	Measured Power Penalty (dB)	Bandwidth-Distance Product (Gb-km/s)
1	10	17	0	10
2	10	34	0	20
5	10	85	0	50
10	10	170	0	100
15	10	255	0	150
40	10	680	0	400
60	10	1020	0.6	600
80	10	1360	2.5	800
80	12.5	1360	2.5	1000

Fig. 6. Summary of experimentally-measured results for varying propagation distances through standard single-mode optical fiber, induced chromatic dispersions, and bandwidth-distance products, of an optical signal encoded using the using the silicon microring resonator electro-optic modulator for modulation rates between 10 and 12.5 Gb/s.

distances through SSMF. We perform BER measurements at the 10-Gb/s modulation rate for each propagation distance configuration (Fig. 5a). For each configuration, error-free operation is initially observed. BER curves are then recorded for the 0-, 1-, 2-, 5-, 10-, 15-, 40-, 60-, and 80-km propagation distances (Fig. 5a). Setting the configuration bypassing the SSMF as the back-to-back case, the measured power penalty is recorded for each propagation distance (Fig. 5b). Compared to the 0-km propagation distance, the measured power penalties remain constant at 0 dB for all propagation distances up to 40 km, and are 0.6- and 2.5-dB for propagation distances of 60 and 80 km, respectively, at the BER of 10^{-9} (Fig. 5b). Using the chromatic dispersion for a given propagation distance characteristic of the SSMF employed in these measurements, which is about 17 ps/(nm-km) at the 1565-nm operating wavelength, the measured power penalties remain constant at 0 dB for all induced chromatic dispersions up to 680 ps/nm, and are 0.6 and 2.5 dB for induced chromatic dispersions of 1020 and 1360 ps/nm, respectively, at the BER of 10^{-9}.

We then record BER curves at the 12.5-Gb/s modulation rate for the 0- and 80-km propagation distances (Fig. 5a). Once again, setting the configuration bypassing the SSMF as the back-to-back case produces a 2.5-dB power penalty. The measured power penalty for each bandwidth-distance product configuration is then determined, producing power penalties that, for the 10-Gb/s modulation rate, remain constant at 0 dB for all bandwidth-distance products up to 400 Gb-km/s, and are 0.6 and 2.5 dB for bandwidth-distance products of 600 and 800 Gb-km/s, respectively. For the 12.5-Gb/s modulations rate, the data signal incurs a 2.5-dB power penalty for the 1000 Gb-km/s bandwidth-distance product. These experimental results are summarized in Fig. 6.

6. Conclusion

Using BER and power penalty characterizations, we have demonstrated a silicon microring resonator electro-optic modulator with error-free transmission for modulation rates up to 12.5 Gb/s. We observed the effects on signal integrity with a varying modulation rate, quantifying the relationship between modulation rate and system-level performance. We then performed a system-level comparative analysis of the silicon modulator using a commercial $LiNbO_3$ Mach-Zehnder electro-optic modulator.

Furthermore, we have also experimentally demonstrated error-free long-haul transmission of optical signals modulated using the silicon modulator, obtaining a bandwidth-distance product up to 1000 Gb-km/s with an 80-km propagation distance and 12.5-Gb/s modulation rate. We characterized the effects of the induced chromatic dispersion on signal integrity, measuring less than a 1-dB power penalty for optical signals modulated at 10 Gb/s and

#129651 - $15.00 USD Received 7 Jun 2010; revised 28 Jun 2010; accepted 28 Jun 2010; published 7 Jul 2010

propagated through 60 km of SSMF. We also reported the resulting power penalties for varying propagation distances up to 80 km, induced chromatic dispersions up to 1360 ps/nm, and bandwidth-distance products up to 1000 Gb-km/s.

Quantifiable performance metrics extracted from experimental validation of silicon photonic devices aid in determining the functionality that these devices perform in large-scale photonic network architectures. We demonstrate that this silicon modulator is truly a versatile silicon photonic device, capable of enabling high-performance transmission for a wide range of short-, medium-, and long-haul applications.

Acknowledgements

We acknowledge support from the National Science Foundation and Semiconductor Research Corporation under grant ECCS-0903406 SRC Task 2001. This work was part of the Interconnect Focus Center Research Program, supported in part by MARCO, Structured Materials Inc. under Grant 41594, National Science Foundation CAREER Program under grant 0446571, and Air Force Office of Scientific Research under grant FA9550-07-1-0200 under the supervision of Dr. Gernot Pomrenke. This work was performed in part at the Cornell NanoScale Facility, a member of the National Nanotechnology Infrastructure Network, which is supported by the National Science Foundation under grant ECS-0335765.

#129651 - $15.00 USD Received 7 Jun 2010; revised 28 Jun 2010; accepted 28 Jun 2010; published 7 Jul 2010